JOURNAL OF APPLIED CRYSTALLOGRAPHY
ISSN 1600-5767

Polarized X-ray diffraction anomalous near-edge structure study on the orbital physics of thin WSe_2 layers

Shih-Lun Chen,[a] Tai-Sing Wu,[b] Hung-Lung Huang,[a] Sheng-Fu Chen,[a] Yun-Liang Soo,[a,b] Horng-Tay Jeng[a,c,d] and Hsueh-Hsing Hung[a]*

[a]Department of Physics, National Tsing Hua University, Hsinchu 30013, Taiwan, [b]National Synchrotron Radiation Research Center, Hsinchu 30076, Taiwan, [c]Physics Division, National Center for Theoretical Sciences, Taipei 10617, Taiwan, and [d]Institute of Physics, Academia Sinica, Taipei 11529, Taiwan. *Correspondence e-mail: hhh@phys.nthu.edu.tw

Received 26 May 2023
Accepted 29 January 2024

Edited by S. Boutet, SLAC National Accelerator Laboratory, Menlo Park, USA

Keywords: diffraction anomalous near-edge structure; polarized DANES; valence orbital structures; 2D transition metal dichalcogenides; 2D TMDC.

Supporting information: this article has supporting information at journals.iucr.org/j

The electronic structures at band edges play an important role in the physical properties of few-layer and monolayer WSe_2. In this study, polarization-dependent diffraction anomalous near-edge structure (DANES) is applied to measure and analyse the electronic orbitals of few-layer WSe_2. By selecting diffraction geometries with the electric field perpendicular or parallel to the c axis of few-layer WSe_2, this method can separately probe the in-plane and out-of-plane orbital components involved at the band edges. The WSe_2 (00.8) surface normal was aligned and the preferred orientation of few-layer WSe_2 grown on an Al_2O_3 (00.1) substrate was identified. DANES was then performed for Se K-edge WSe_2 00.8 and 11.0 reflections to examine the W 5d orbitals hybridized with the Se 4p orbitals: these two DANES spectra exhibit fairly anisotropic valence orbital characteristics in few-layer WSe_2. Coupled with first-principles calculations, these results allow the identification of the in-plane and out-of-plane orbital distribution and hybridization in WSe_2. At the conduction band edge, the contributions of p_x and p_y orbitals are predominant over p_z and the splitting of the p-orbital energy levels has been confirmed. Hence DANES is shown to be a useful synchrotron X-ray technique that can help identify the valence orbital structure of various 2D transition metal dichalcogenides.

1. Introduction

Two-dimensional transition metal dichalcogenides (TMDCs, MX_2: M = W and Mo; X = S, Se, Te) have attracted wide attention in recent years because of their unique characteristics for developing new generation semiconductor and optoelectronic devices, as well as their photocatalytic applications. The tunability of TMDC materials has resulted in astonishing electronic and optical properties. For instance, the band gap adapts with the material thickness going from bulk to few- or monolayer TMDCs, and spin-valley coupling occurs due to a parity symmetry breaking. Further, Moiré patterns with twisted TMDC homo- or heterostructures lead to superconducting phases or the formation of topological insulators (An *et al.*, 2020; Tong *et al.*, 2017). Nowadays, researchers utilize various techniques to study the electronic structures of 2D TMDC materials. For example, by employing circularly polarized photoluminescence spectra (Jones *et al.*, 2014), spin-valley coupling and behaviour of excitons in 2D materials can be detected. Angle-resolved photoemission spectroscopy can even investigate the electronic band structure directly (Jin *et al.*, 2013). Meanwhile, the structure of the valence orbitals around the band edge is also an important issue in research. By tuning the strain, doping or heterostructure fabrication

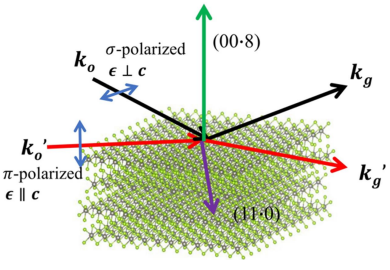

methods, the orbital distribution at band edges will change greatly and bring about novel physical properties (Amin *et al.*, 2016; Chae *et al.*, 2017; Miao *et al.*, 2020). For example, MoS_2–WSe_2 heterostructures have distinct Mo and W orbital distributions at the band edges. Adding strain to the heterostructure WS_2–$MoSe_2$ also changes the band gap from indirect to direct and alters the orbital contributions. V-doped and undoped monolayer MoS_2 have different magnetic properties due to the different orbital structures (Miao *et al.*, 2020). To deepen our understanding of the electronic and crystal structures of thin TMDCs, here we employed polarization-dependent DANES to study the electronic orbital structure of these materials near the band edges.

DANES, like diffraction anomalous fine structure and resonant X-ray scattering, is a synchrotron-based X-ray technique that couples X-ray diffraction with X-ray absorption spectroscopy (XAS). At a specific absorption edge, it probes the unoccupied valence electronic structure and local chemical environment around selected elements in a specific crystalline phase (Stragier *et al.*, 1992). The anomalous scattering occurs around the absorption edge through a transition process of core-level electrons excited to unoccupied states above the valence band edge. Therefore, the atomic scattering factor should be modified by $f' + if''$, where f' and f'' are the real and imaginary parts of the atomic anomalous scattering factor, respectively. The structure factor for a given reflection can be written as

$$F\exp(i\delta) = \sum_{a(\mathrm{res})}\left(f_a^0 + f_a' + if_a''\right)\exp(2\pi i\mathbf{g}\cdot\mathbf{r}_a) + \sum_b f_b^0\exp(2\pi i\mathbf{g}\cdot\mathbf{r}_b). \quad (1)$$

The symbols a and b represent resonantly excited atoms and non-resonant atoms at the absorption edge of interest, respectively. $\mathbf{g}$ is the diffraction vector, $\mathbf{r}_a$ and $\mathbf{r}_b$ are atomic position vectors, and f_0 is the Thomson atomic scattering factor. By analysing the profile of diffraction intensity at various X-ray energies, the spectrum provides site-specific information due to, for example, charge separation, orbital ordering and structural transformations (Ueda *et al.*, 2021; Grenier *et al.*, 2018). Mostly, by considering the atomic anomalous scattering factor in tensor form (Bunău, 2010), DANES is very sensitive to the local environment of the target atoms. The direction of polarization can be specified at a specific diffraction. Therefore, polarization-dependent DANES not only probes the density of states but can also separate different orbital components due to the linear polarization of synchrotron X-rays. Namely, it can resolve the orbital structures near the band gap along either the in-plane or the out-of-plane direction under a specified polarization arrangement. Besides, DANES has two advantages over polarization-dependent XAS. First, DANES can probe a specific domain or crystalline phase under a certain diffraction condition from a multi-domain or multi-phase sample. Further, by employing grazing-incidence X-ray diffraction, DANES becomes sensitive to the surface and/or interfacial properties of composite materials, such as bilayer heterostructures or twist-angle structures, which is crucial to investigate interlayer coupling in TMDC materials.

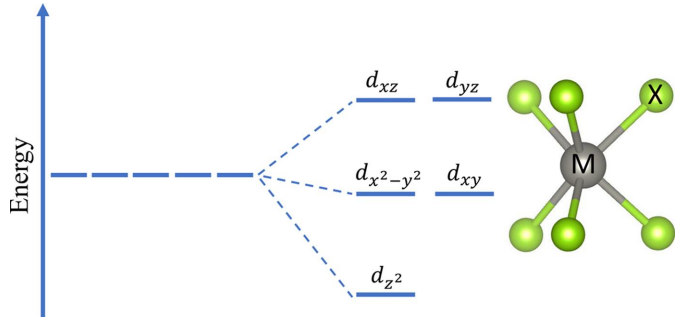

Figure 1
According to the tight-binding model, the crystal field effect on WSe_2 causes the 5*d* orbital of *W* to split into three energy levels: d_{xz} and d_{yz} (topmost), $d_{x^2-y^2}$ and d_{xy} (middle), and d_{z^2} (bottom). The valence charges are considered by filling the occupied d_{z^2} state.

Layered WSe_2 exhibits a hexagonal symmetry with a honeycomb structure that usually constitutes trigonal prismatic bonding coordination (2H). It belongs to the $P6_3/mmc$ space group (Traving *et al.*, 1997). Because of the crystal field effect in such transition metal compounds, the energy level of the W 5*d* orbital will split into d_{xz} and d_{yz} (topmost), $d_{x^2-y^2}$ and d_{xy} (middle), and d_{z^2} (bottom) (Gong *et al.*, 2013), as shown in Fig. 1. According to ligand field theory, W 5*d* hybridizes with Se 4*p* orbitals in the outer shell which determines the electronic structure. The number of layers in WSe_2 will also affect the orbital distribution around the edge of conduction and valence bands (Yazyev & Kis, 2015).

In this work, a polarization-dependent DANES study of few-layer WSe_2 is applied to analyse the orbital hybridization of W 5*d* with Se 4*p*. Anisotropic features of DANES spectra for polarization along the in-plane versus out-of-plane direction have been resolved. By employing first-principles calculations based on density functional theory (DFT), we obtain results (such as lattice parameters and bond lengths) that are in good agreement with previous research and which support the observed spectra satisfactorily.

2. Experimental setup and theoretical work

The sample of few-layer WSe_2 was deposited on a 10 × 10 mm sapphire substrate through chemical vapour deposition. Both X-ray scattering and DANES measurements were carried out on beamlines TLS-17B1, TLS-07A1 and TPS-09A1 at the National Synchrotron Radiation Research Center (NSRRC). The incident X-ray beam was energy-tuned by an Si(111) double-crystal monochromator (DCM). The incident X-ray was then collimated by a horizontal focusing mirror which guided the X-ray to the sample at the centre of diffractometer.

Figs. 2(*a*) and 2(*b*) illustrate the setup for measurements of few-layer WSe_2 in the polarized DANES method, referring to the Se *K* edge at 12658 eV with energies scanned from 12610 to 12710 eV. In four-circle diffractometry mode with the χ angle set at −90°, we measured the surface-normal (00.*l*) diffraction along the *c* axis of the WSe_2 sample. The in-plane

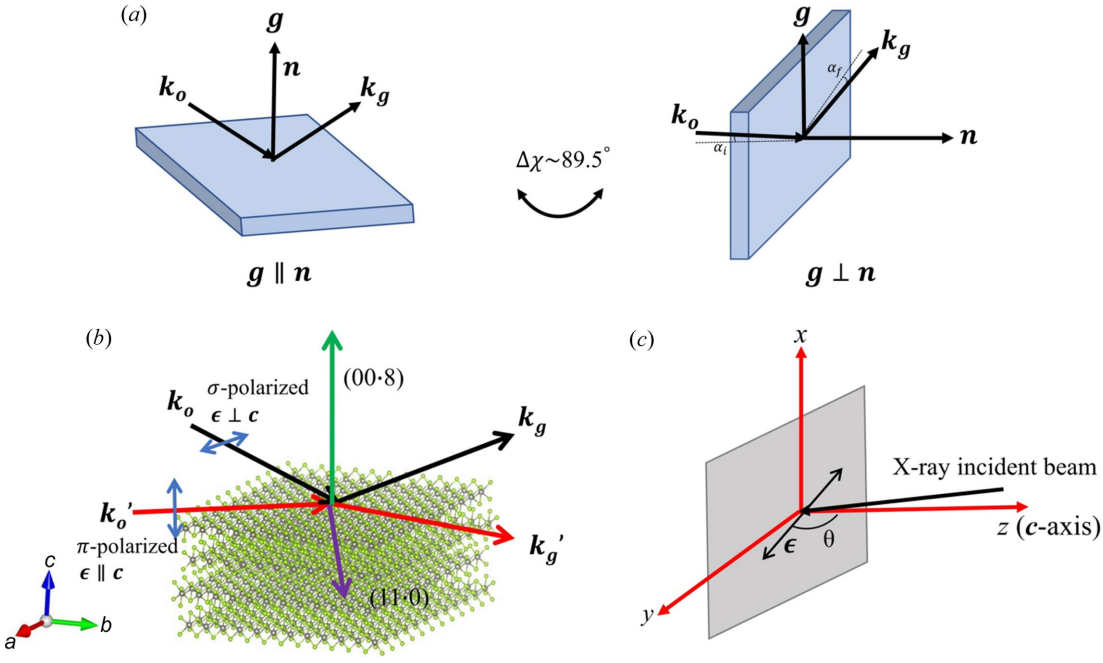

Figure 2
(*a*) Scattering geometry of the surface-normal diffraction with $\mathbf{g} \parallel \mathbf{n}$ versus the in-plane diffraction with $\mathbf{g} \perp \mathbf{n}$. (*b*) Schematic of the polarization-dependent DANES measurements. (00.8) and (11.0) represent the scattering beams with σ- and π-polarization, respectively. (*c*) Geometry of angle-dependent X-ray absorption spectroscopy to study the anisotropy of samples.

(*hk*.0) diffraction was then performed by fixing χ at -0.5°. In the grazing-incidence geometry, the reciprocal lattice vector $\mathbf{g}$ of (*hk*.0) is perpendicular to the surface normal $\mathbf{n}$. The incident angle α_i to the crystal surface was set at 0.3°, and the outgoing angle α_f was estimated as 0.3° as well.

According to the structure factor, the 00.8 and 11.0 reflections are good candidates for DANES measurements. The scattering geometry of (00.8) diffraction, shown in Fig. 2(*b*), is in σ-polarization. Namely, the electric field of the X-rays is perpendicular to the surface normal $\mathbf{n}$ (that is, the *c* axis) of the sample. In contrast, the in-plane diffraction (11.0) diffraction involves π-polarization, with the electric field of the scattered beam parallel to the *c* axis. Polarization-dependent DANES is conceptually consistent with angle-dependent X-ray absorption spectroscopy (Brouder *et al.*, 2008; Rossi *et al.*, 2019) by rotating the sample around its *x* axis, as shown in Fig. 2(*c*), so that the angle θ between the electric field of the incident X-rays and the surface normal of the sample varies from $\theta = 0^\circ$ ($\boldsymbol{\epsilon}$ parallel to the *c* axis) to $\theta = 90^\circ$ ($\boldsymbol{\epsilon}$ perpendicular to the *c* axis).

In the theoretical part of this work, finite difference method near-edge structure (*FDMNES*) code (Joly, 2001) and the Vienna *ab initio* simulation package (*VASP*) (Kresse & Furthmüller, 1996) were used to calculate the electronic structure of few-layer WSe_2. The *FDMNES* code is widely applied to simulate DANES and X-ray absorption near-edge structure (XANES) spectra. Theoretically, the atomic anomalous scattering factor can also be written as (Joly *et al.*, 2018)

$$f_j' - if_j'' = m\omega^2 \sum_{\mathrm{g}} \sum_{\mathrm{f}} \frac{\langle \psi_{\mathrm{g}} | \mathbf{o}_{\mathrm{s}}^* | \psi_{\mathrm{f}} \rangle \langle \psi_{\mathrm{f}} | \mathbf{o}_{\mathrm{i}} | \psi_{\mathrm{g}} \rangle}{\hbar\omega - \left(E_{\mathrm{f}} - E_{\mathrm{g}}\right) + i[\Gamma(E)/2]}. \quad (2)$$

The imaginary part f_j'' is also proportional to the X-ray absorption spectrum in which the absorption cross section σ_{R} can be written as

$$\sigma_{\mathrm{R}} = 4\pi^2 \alpha \hbar\omega \sum \left| \langle \psi_{\mathrm{f}} | \mathbf{o}_{\mathrm{i}} | \psi_{\mathrm{g}} \rangle \right|^2 \delta\left(E_{\mathrm{f}} - E_{\mathrm{g}} - \hbar\omega\right), \quad (3)$$

where $\alpha = e^2/(2hcE_0)$ and $\mathbf{o}_{\mathrm{i}}$ and $\mathbf{o}_{\mathrm{s}}$ are operators of the incoming and outgoing X-ray beams describing the interaction of the electromagnetic field with matter and constituting the transition matrix. The operators can be expressed as

$$\mathbf{o}_n \simeq \boldsymbol{\epsilon}_n \cdot \mathbf{r} + \frac{i}{2}(\boldsymbol{\epsilon}_n \cdot \mathbf{r})(\mathbf{k}_n \cdot \mathbf{r}). \quad (4)$$

Here we only consider the dipole and quadrupole transitions, where $\boldsymbol{\epsilon}_n$ is the electric field and $\mathbf{k}_n$ is the wavevector of the X-rays (n = i or s). In anomalous scattering, electrons in the core state ψ_{g} will be excited to the intermediate state ψ_{f} (the final state for X-ray absorption) for a finite time and then relax back to the core hole, described by the energy-dependent broadening $\Gamma(E)$. In particular, equation (4) tells us that both the polarization and the wavevector of the electromagnetic waves play a key role in determining the final density of the state probed.

3. Results and discussion

Fig. 3(*a*) shows a surface-normal diffraction (00.8) 2θ–θ scan of few-layer WSe_2 at 12660 eV, where two components were observed in the scattering profile. The Voigt function was applied to fit these two components. The resulting fits, with peaks located at $2\theta = 34.999^\circ \pm 0.216^\circ$ and $33.157^\circ \pm 0.750^\circ$, are depicted as red and green solid curves, respectively. The blue solid curves are the sum of the red and green solid curves.

The corresponding interlayer correlation lengths are 5.2 nm (±0.2 nm) for the high-angle peak and 1.5 nm (±0.3 nm) for the low-angle peak from the Scherrer equation. In the in-plane 2H-WSe_2 (11.0) diffraction profile at 12610 eV, as shown in Fig. 3(*b*), there are also two peaks located at $2\theta = 34.768^\circ \pm 0.033^\circ$ and $34.945^\circ \pm 0.034^\circ$, as shown in the two-component

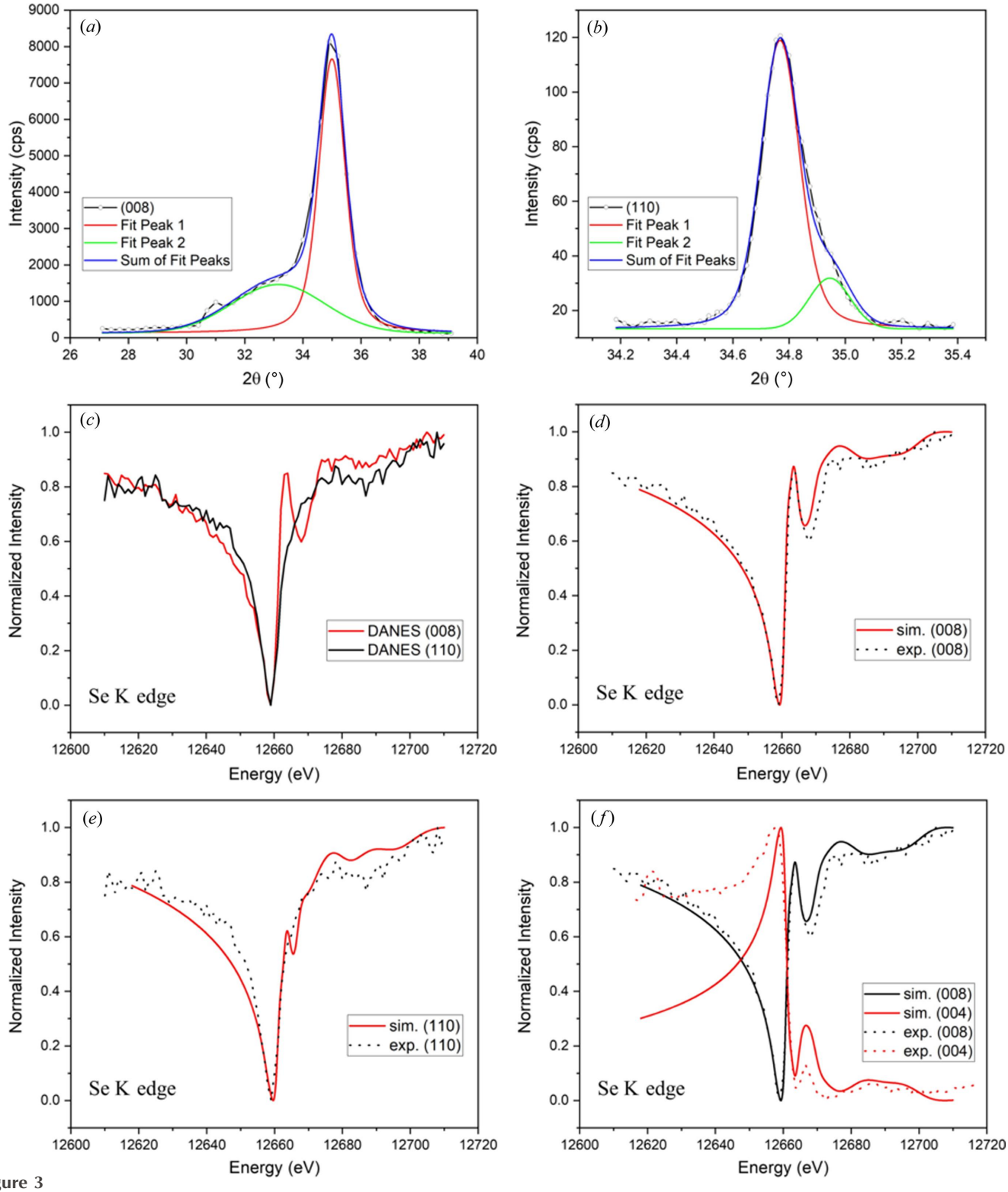

Figure 3
Characterization of few-layer WSe_2 in X-ray scattering and polarization-dependent DANES measurements. Diffraction profiles of the 2θ–θ scan for (*a*) surface-normal and (*b*) in-plane diffraction. (*c*) Experimental DANES spectra for 00.8 (red line) and 11.0 (black line). Simulated DANES spectra (red line) derived from the *FDMNES* code are compared with experimental DANES spectra (black dotted line) for (*d*) 00.8 and (*e*) 11.0. (*f*) Simulated DANES spectra of the 00.8 and 00·4 reflections compared with the experimental results at the same σ-polarization.

fitting curve. The lattice mismatch between 2H-WSe_2 and the sapphire substrate introduces compressive strain so as to reduce the lateral lattice parameter a of WSe_2. Thus, the weak-intensity component (green curve) is attributed to a bottom layer with a smaller a = 3.27 Å (±0.003 Å). The strong-intensity component (red curve) with the lattice parameter a = 3.29 Å (±0.003 Å) is attributed to the WSe_2 top layers which are less influenced by the substrate. The lateral correlation lengths from this major peak (34.768°, red curve) and the weak peak (34.945°, green curve) are determined to be about 35 nm (±1 nm) and 32 nm (±5 nm), respectively. Correspondingly, the compressed strain caused the lattice parameter c of the WSe_2 bottom layer to increase. In the case of surface-normal diffraction, the weak peak at the low angle 2θ = 33.157° is mainly attributed to the bottom layer; however, the major peak at 2θ = 34.999° is associated with the top layer. The lattice parameters in the bottom and top layers were obtained as c = 13.73 Å (±0.30 Å) and c = 13.03 Å (±0.08 Å), respectively. Consequently, the two major peaks from the (00.8) and (11.0) diffraction profiles were utilized to perform the following DANES measurements.

In the DANES measurements of the 00.8 and 11.0 reflections, 2θ is located at the centre of each peak to keep the scattering vector **q** of WSe_2 00.8 and 11.0 fixed when scanning the X-ray energy of the incident beam (see the supporting information). The energy resolution of the incident X-rays from the DCM is better than 2×10^{-4} at 12658 eV, and the corresponding incident-beam divergence angle is about 0.002°. This energy resolution is appropriate to conduct DANES measurements so as to resolve the energy spectrum of a specific crystalline phase. In Fig. 3(*c*), DANES spectra of the WSe_2 00.8 and 11.0 reflections exhibit quite different features under each specific selection of the polarization. According to the DANES of the 00.8 reflection, there is a sharp resonance identified at 12663 eV which indicates a particular spectral weight of the p orbital above the edge; however, this feature is filtered out in the DANES of the 11.0 reflection. To analyse these DANES data, theoretical computation was implemented in the *FDMNES* code. The finite difference method in an exchange-correlation potential introduced by Hedin, Lundqvist and Von Barth was applied. A cluster of radius 6.95 Å was built, centred at the Se atom and taking 69 atoms into account, to obtain simulated DANES and XANES spectra. The spectrum from the cluster of radius 6.95 Å is compared with those for 5 and 7.1 Å radii, showing that the features of the spectra at 6.95 and 7.1 Å are nearly unchanged (see the supporting information). Hence, our calculations can be considered convergent. Both the relativistic and the spin-orbit coupling (SOC) effect were taken into account without the Hubbard U correction. The fractional atomic coordinates are listed in the supporting information. The intensity of simulated DANES spectra can be derived after the calculation of the real and imaginary parts of the anomalous atomic scattering factor. The simulated XANES spectra are obtained in units of absorption cross section (in MBarn). The simulated XANES, simulated DANES and experimental DANES spectra were normalized so that the minimum and the maximum of the spectrum are 0 and 1, respectively. From Figs. 3(*d*) and 3(*e*), the simulated DANES spectra of the 00.8 and 11.0 reflections are roughly in agreement with experimental data.

Table 1
Structure parameters of few-layer WSe_2 obtained from experiments (first row) are compared with theoretical calculations of bulk (second row) and monolayer (sixth row) WSe_2.

The previous theoretical and experimental results are also listed.

	a (Å)	b (Å)	c (Å)	W—Se (Å)	E_g (eV)	Pseudopotential types
Experiment	3.29	3.29	13.03			
Bulk	3.308	3.308	13.607	2.543	1.05	GGA, SOC
Theoretical†	3.299	3.299	13.092			GGA+D, non-SOC
Experiment‡	3.282	3.282	12.960	2.526		
Experiment§	3.290	3.290	12.970		1.42	
Monolayer	3.311	3.311		2.544	1.54	GGA, SOC
Theoretical¶	3.29	3.29		2.541	1.61	GGA, non-SOC

† Feng *et al.* (2014). ‡ Schutte *et al.* (1987). § Delphine *et al.* (2003). ¶ Yang *et al.* (2016).

To examine the simulated DANES spectrum of the 00.8 reflection calculated by *FDMNES*, the DANES spectrum of the 00.4 reflection is also calculated and shown in Fig. 3(*f*). For both measured and simulated DANES spectra, the main feature around the absorption edge looks similar. Though the DANES spectra of the 00.8 and 00.4 reflections have the same polarization (*i.e.* the electric field of X-rays perpendicular to the c axis), resulting from the phase change of the anomalous scattering factor of the selected element between the 00.8 and 00.4 reflections, the discrepancy is apparent.

In the simulated DANES spectrum of the 11.0 reflection, there is a short dip at 12663 eV, but only a shoulder is observed from the measurement. This dissimilarity might be caused by several factors, for instance, the intensity being too low as the diffraction geometry is set at grazing incidence, the lack of resolution power of the experimental instrument and various defects from the crystalline quality of the sample. Note that the dip has the same amplitude as the noise level, which can be estimated from the fluctuations in the background between 12620 and 12710 eV. These fluctuations might be the main factor that explains why we did not observe such a dip feature in the experiment. Nevertheless, the similarities indicate that the *FDMNES* code is reliable enough to analyse our DANES data.

To analyse the DANES spectra with respect to the near-edge electronic structure of orbital hybridization, the partial density of states (pDOS) of WSe_2 was calculated on the basis of DFT as implemented in the *VASP* code. The PBE-type generalized gradient approximation (Perdew & Wang, 1992) was adopted for the exchange and correlation effects. A Gamma-centred Monkhorst–Pack k-mesh of 15 × 15 × 3 was used in the first Brillouin zone integration with a cut-off energy of 400 eV. In the self-consistent calculation, the total energy convergence condition was set to 1×10^{-6} eV. The fully optimized structure was obtained when the total energy converges within 1×10^{-5} eV. Supercell approximation was used to simulate the structure of monolayer WSe_2 under a

k-mesh of 15 × 15 × 1. The vacuum thickness was set to 20, which was large enough to eliminate interactions between periodic layers.

Table 1 shows our calculated structure parameters and the band gap for bulk and monolayer WSe_2 in comparison with other theoretical and experimental results. The calculated bulk lattice parameters a (3.308 Å) and c (13.607 Å) are 0.54 and 4.67% larger than the experimental values reported by Delphine *et al.* (2003), whereas the W—Se bond length (2.543 Å) is only 0.67% larger than the experimental one. For the monolayer, the calculated lattice constants (a = 3.311 Å) and the bond length of W—Se (2.544 Å) are 0.63 and 0.12% larger than previous theoretical calculations. This shows that our calculated structure parameters are close to previous results. Therefore, we believe that the DFT-GGA calculation is reasonable and can be used to explain the experimental results in this study.

The simulated XANES, simulated DANES and experimental DANES spectra, shown in Figs. 4(*a*) and 4(*b*), are compared with the calculated pDOS of bulk WSe_2 with the SOC effect, shown in Figs. 4(*c*) and 4(*d*), where the W 5*d* and Se 4*p* pDOS are projected along in-plane (perpendicular to the c axis) and out-of-plane (parallel to the c axis) directions, respectively. Both the valence band maximum and conduction band minimum are mainly composed of W d_{z^2}, $d_{x^2-y^2}$ and d_{xy}. While W d_{xz} and d_{yz} contribute primarily to the energy region [−1, −4] eV. pDOS also reveals that W $d_{x^2-y^2}$–d_{xy}, W d_{xz}–d_{yz} and Se p_x–p_y are degenerate. Here, we focus on investigating pDOS above the Fermi level (zero point) corresponding to XANES and DANES spectra after the absorption edge 12658 eV. From Fig. 4(*a*), according to equations (2)–(4), both the XANES measurement and the DANES spectrum of the 00.8 reflection probe the in-plane orbitals Se p_x and p_y due to the σ-polarization (the electric field perpendicular to the c axis) under the excitation of electrons from 1*s* to 4*p*. Further, in Fig. 4(*c*), the pDOS profiles of Se p_x and p_y overlap, as do those of W $d_{x^2-y^2}$ and d_{xy}, demonstrating related distributions from 1.4 to above 10 eV. In particular, the distributions of pDOS of p_x and p_y are more localized from 1.4 to 4.2 eV like W $d_{x^2-y^2}$ and d_{xy}. The in-plane pDOS of W *d* as well as that of Se *p* possesses a strong peak at $E - E_F$ = 2.3 eV, where E_F is the Fermi energy. These results show that there is an apparent orbital hybridization along the in-plane direction. Therefore, we infer that the DANES spectrum of the 00.8 reflection probes not only Se p_x and p_y but also W $d_{x^2-y^2}$ and d_{xy}, which brings about the observed sharp peaks at 12663 eV.

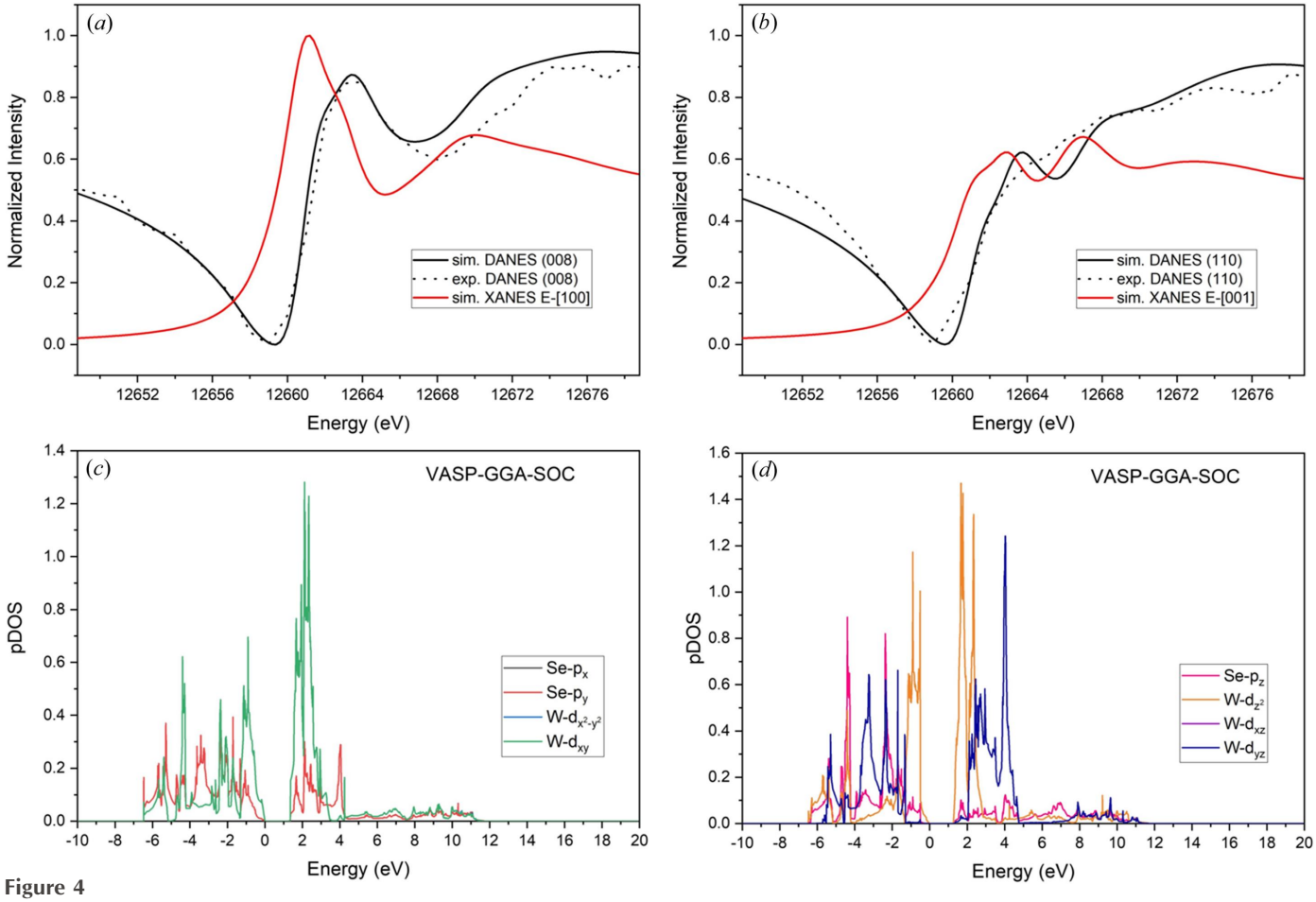

Figure 4
DANES and polarization-dependent XANES spectra for (*a*) in-plane polarization DANES 00.8 and (*b*) out-of-plane polarization DANES 11.0 are examined by the DFT calculation of the projected partial density of states of the corresponding bulk WSe_2 in (*c*) and (*d*). Dotted lines are the experimental DANES spectra, and black and red solid lines are the simulated DANES and XANES spectra, respectively.

From Fig. 4(*b*), both the XANES measurement and the DANES of the 11.0 reflection probe out-of-plane orbitals under π-polarization (the electric field parallel to the *c* axis). These spectra do not show any noticeable peaks like those seen in Fig. 4(*a*). Comparing the pDOS of WSe_2 along the out-of-plane direction shown in Fig. 4(*d*), the pDOS of Se p_z is on average lower than 0.15 in contrast to those of W d_{z^2}, d_{xz} and d_{yz}, which are larger than 1.2. The distribution of pDOS of Se p_z is not localized (in contrast to W d_{z^2}, d_{xz} and d_{yz}, which spread mostly from 1.2 to 5 eV). It exhibits a typical extended feature spanning from 1.2 to 11.1 eV. These findings indicate that the orbital hybridization is weaker along the out-of-plane direction, where the XANES measurement and the DANES of the 11.0 reflection mainly probe the Se p_z orbital so that the only feature is a bump in these spectra.

As a result, both experimental data and theoretical work demonstrate that the crystal field effect influences the interaction and hybridization of W 5*d* and Se 4*p* orbitals. We observed that the pDOS features of p_x and p_y apparently differ from those of p_z. This result confirms that, due to the crystal field effect, the energy spectrum of *p* orbitals splits into p_x–p_y degeneracy and p_z. This effect also implies that the contribution of p_z spectral weight is less than that of p_x and p_y at the conduction edge.

4. Conclusions

In this work, we applied polarization-dependent DANES to study the orbital physics of few-layer WSe_2. The compressive strain due to the sapphire substrate resulted in lattice deformation of few-layer WSe_2 such that two components of diffraction were observed. We chose the less-strained top layer to perform DANES measurements. The surface-normal and in-plane DANES spectra showed distinct features. With the excitation at the Se *K* edge of WSe_2, we analysed the unoccupied state of the Se 4*p* orbital and W 5*d* orbital hybridization under the crystal field effect. In the theoretical work, DFT calculations presented the broken degeneracy of W 5*d* and Se 4*p* orbitals, bringing about the different orbital distribution. Coupled with DFT results, the features of two DANES spectra reveal that the in-plane orbital hybridization is prevalent at the band edge. Nevertheless, hybridization along the out-of-plane direction is weak. The results show that van der Waals layered materials break the symmetry of charge distribution under the crystal field effect, leading to anisotropic orbital hybridization. The polarization-dependent DANES in this work demonstrates the capability of probing specific crystalline structures to directly resolve the orbital hybridization. This technique is promising in its application to the study of the near-edge electronic structure of 2D materials processed using various methods, such as the growth of thin films on different substrates, and the fabrication of hetero- or twisted-angle structures.

Acknowledgements

We express our gratitude to the beamline staff at NSRRC for their assistance. SLC and H-HH would like to thank the anonymous referee for his kind and thorough comments on and suggestions for this manuscript.

Funding information

This research was financially supported by the National Science Council of Taiwan (grant No. MOST 110–2112-M007-039; MOST 109–2112-M-007–034-MY3). HTJ also thanks the NCHC, CINC-NTU, AS-iMATE-109-13 and CQT-NTHU-MOE, Taiwan, for support.

References

Amin, B., Kaloni, T. P., Schreckenbach, G. & Freund, M. S. (2016). *Appl. Phys. Lett.* **108**, 063105.
An, L., Cai, X., Pei, D., Huang, M., Wu, Z., Zhou, Z., Lin, J., Ying, Z., Ye, Z., Feng, X., Gao, R., Cacho, C., Watson, M., Chen, Y. & Wang, N. (2020). *Nanoscale Horiz.* **5**, 1309–1316.
Brouder, C., Juhin, A., Bordage, A. & Arrio, M. (2008). *J. Phys. Condens. Matter*, **20**, 455205.
Bunău, O. (2010). PhD thesis, Université de Grenoble, France.
Chae, W. H., Cain, J. D., Hanson, E. D., Murthy, A. A. & Dravid, V. P. (2017). *Appl. Phys. Lett.* **111**, 143106.
Delphine, S. M., Jayachandran, M. & Sanjeeviraja, C. (2003). *Mater. Chem. Phys.* **81**, 78–83.
Feng, L.-P., Li, N., Yang, M.-H. & Liu, Z. (2014). *Mater. Res. Bull.* **50**, 503–508.
Gong, C., Zhang, H., Wang, W., Colombo, L., Wallace, R. M. & Cho, K. (2013). *Appl. Phys. Lett.* **103**, 053513.
Grenier, S., Bailly, A., Ramos, A. Y., De Santis, M., Joly, Y., Lorenzo, J. E., Garaudée, S., Frericks, M., Arnaud, S., Blanc, N. & Boudet, N. (2018). *Phys. Rev. B*, **97**, 104403.
Jin, W., Yeh, P.-C., Zaki, N., Zhang, D., Sadowski, J. T., Al-Mahboob, A., van der Zande, A. M., Chenet, D. A., Dadap, J. I., Herman, I. P., Sutter, P., Hone, J. & Osgood, R. M. (2013). *Phys. Rev. Lett.* **111**, 106801.
Joly, Y. (2001). *Phys. Rev. B*, **63**, 125120.
Joly, Y., Abisset, A., Bailly, A., De Santis, M., Fettar, F., Grenier, S., Mannix, D., Ramos, A. Y., Saint-Lager, M. C., Soldo-Olivier, Y., Tonnerre, J. M., Guda, S. A. & Gründer, Y. (2018). *J. Chem. Theory Comput.* **14**, 973–980.
Jones, A. M., Yu, H., Ross, J. S., Klement, P., Ghimire, N. J., Yan, J., Mandrus, D. G., Yao, W. & Xu, X. (2014). *Nat. Phys.* **10**, 130–134.
Kresse, G. & Furthmüller, J. (1996). *Comput. Mater. Sci.* **6**, 15–50.
Miao, Y., Bao, H., Fan, W. & Ma, F. (2020). *J. Phys. Chem. Solids*, **142**, 109459.
Perdew, J. P. & Wang, Y. (1992). *Phys. Rev. B*, **45**, 13244–13249.
Rossi, T. C., Grolimund, D., Nachtegaal, M., Cannelli, O., Mancini, G. F., Bacellar, C., Kinschel, D., Rouxel, J. R., Ohannessian, N., Pergolesi, D., Lippert, T. & Chergui, M. (2019). *Phys. Rev. B*, **100**, 245207.
Schutte, W., De Boer, J. & Jellinek, F. (1987). *J. Solid State Chem.* **70**, 207–209.
Stragier, H., Cross, J., Rehr, J., Sorensen, L. B., Bouldin, C. E. & Woicik, J. C. (1992). *Phys. Rev. Lett.* **69**, 3064–3067.
Tong, Q., Yu, H., Zhu, Q., Wang, Y., Xu, X. & Yao, W. (2017). *Nat. Phys.* **13**, 356–362.
Traving, M., Boehme, M., Kipp, L., Skibowski, M., Starrost, F., Krasovskii, E. E., Perlov, A. & Schattke, W. (1997). *Phys. Rev. B*, **55**, 10392–10399.
Ueda, H., Porer, M., Mardegan, J. R. L., Parchenko, S., Gurung, N., Fabrizi, F., Ramakrishnan, M., Boie, L., Neugebauer, M. J., Burganov, B., Burian, M., Johnson, S. L., Rossnagel, K. & Staub, U. (2021). *Phys. Rev. Res.* **3**, L022003.
Yang, C.-X., Zhao, X. & Wei, S.-Y. (2016). *Solid State Commun.* **245**, 70–74.
Yazyev, O. V. & Kis, A. (2015). *Mater. Today*, **18**, 20–30.